

Modeling and Optimization of Vortex Modes Propagation in Rectangular Dielectric Waveguides

Volume 12, Number 1, February 2020

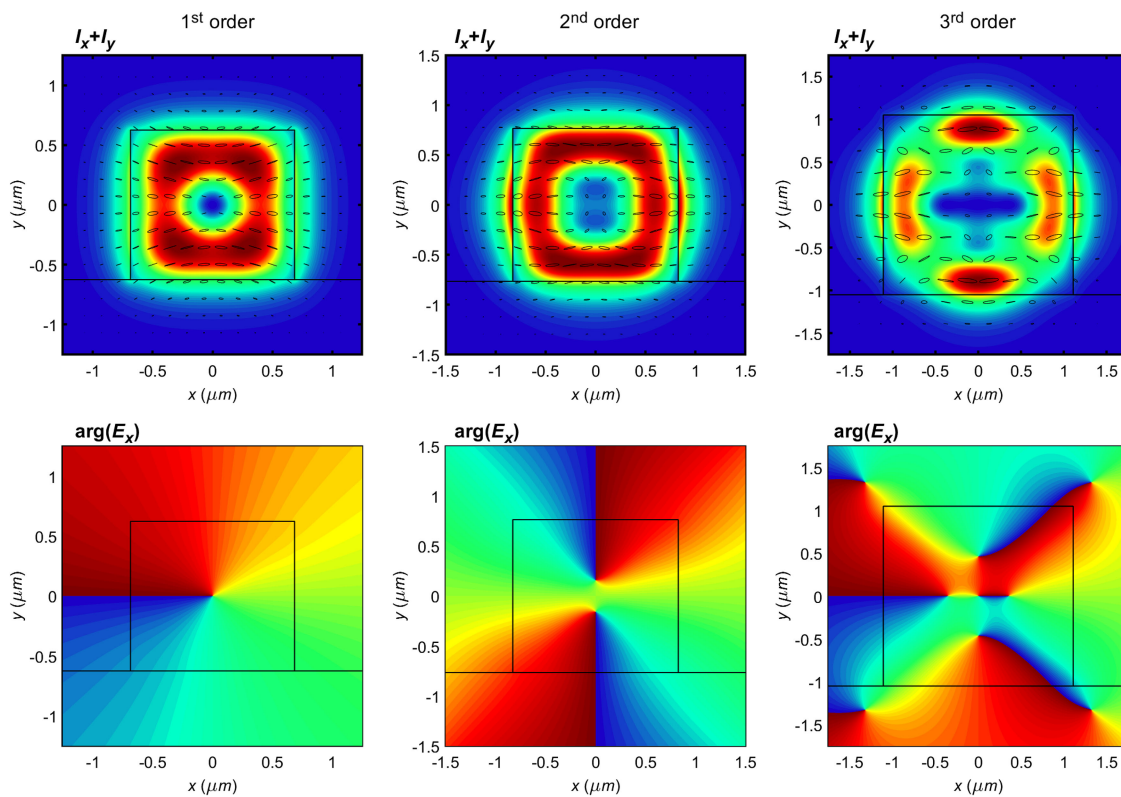
Vladimir S. Lyubopytov, *Member, IEEE*

Ruslan V. Kutluyarov, *Member, IEEE*

Valeriy K. Bagmanov

Niels Neumann

Albert K. Sultanov



DOI: 10.1109/JPHOT.2019.2958273

Modeling and Optimization of Vortex Modes Propagation in Rectangular Dielectric Waveguides

Vladimir S. Lyubopytov ,¹ Member, IEEE,
Ruslan V. Kutluyarov ,¹ Member, IEEE, Valeriy K. Bagmanov ,¹
Niels Neumann ,² and Albert K. Sultanov ,¹

¹Telecommunication Systems Department, Ufa State Aviation Technical University, Ufa
450008, Russia

²Chair for RF and Photonics Engineering, Technische Universität Dresden, 01062
Dresden, Germany

DOI:10.1109/JPHOT.2019.2958273

This work is licensed under a Creative Commons Attribution 4.0 License. For more information, see
<https://creativecommons.org/licenses/by/4.0/>

Manuscript received September 26, 2019; revised November 19, 2019; accepted December 3, 2019.
Date of publication December 9, 2019; date of current version January 7, 2020. This work was funded
under the Grant of the Russian Science Foundation (Project No. 19-49-04112). Corresponding author:
Vladimir S. Lyubopytov (e-mail: lyubopytov.v@gmail.com).

Abstract: We study analytically and numerically the possibility of vortex modes propagation over planar dielectric rectangular waveguides, and consider the problem of waveguide geometry optimization for the support of vortex modes. The results show, that theoretically rectangular waveguides can provide transmission of quasi-TE and quasi-TM modes with high purity states of orbital angular momentum (OAM) in the dominant field component. However, only for the quasi-generate mode of azimuthal order ± 1 the constituent eigenmodes can propagate in a phase-matched regime, and the vortex modes of higher azimuthal orders can propagate only with a certain beat length. Moreover, as the target azimuthal order increases, the normalized power of the corresponding OAM state in the modal superposition decreases. The analytical predictions have been verified by numerical electromagnetic simulations of silicon nitride waveguides providing field distributions and OAM spectra of the corresponding modal superpositions.

Index Terms: Optical orbital angular momentum (OAM), optical waveguides, integrated photonics, silicon nitride.

1. Introduction

Since the time when it was recognized by Allen *et al.* [1] that a helically-phased light beam (commonly referred to as an optical vortex) inherently possesses an orbital angular momentum (OAM) of $\ell\hbar$ per photon (where integer ℓ is the topological charge of vortex beam and \hbar is the Planck constant), voluminous applications of optical vortices have been developed [2], [3]. As OAM can provide theoretically infinite number of states, the utilization of OAM as an additional orthogonal basis of information carriers can enhance tremendously the capacity of both classic optical communications [4], [5] and quantum information systems [6]–[8]. In optical fiber communications, an orthogonal set of OAM modes can be used for mode-division multiplexing (MDM) [9], which is a foreseeable way out of the expected “capacity crunch”, i.e., the exponential growth of the bandwidth demand quickly approaching the nonlinear Shannon limit with state-of-the-art modulation formats [10]. Particularly, in short-range scenarios the use of OAM fiber modes is advantageous due to their ability to withstand unwanted mode coupling, and hence prevent crosstalk between modal channels

[11]–[13]. Moreover, the application areas of optical vortices involve but are not limited to micro particle optical manipulation [14], [15], optical sensors [16], [17], optical imaging and microscopy beyond the diffraction limit [18], [19].

Initially, transmission of optical vortices has been investigated in free space [20]–[27] and optical fibers [11]–[13], [28]–[30]. Usually, in such systems, discrete optical devices, such as diffractive optical elements [6], [20], [21], [28], liquid crystal based spatial light modulators [11], [12], [22]–[26], [30] or specific optical elements [29] are used for generation, control and detection of vortex beams.

More recently, in order to provide miniaturization, robustness, repeatability in massive production, cost and energy efficiency of the systems involving optical vortices, significant attention of research groups has been focused on developing photonic integrated circuits (PICs) for generation, processing and detection of vortex modes. As a result, a number of integrated OAM-based solutions have been proposed, which in general can be subdivided into three groups depending on the approaches used for vortex beam generation and transmission: i) out-of-plane solutions [31]–[44]; ii) in-plane solutions [45]–[49], and iii) solutions based on three-dimensional (3D) PICs [50], [51]. In the current paper, we focus on planar (two-dimensional) waveguides, which are compatible with standard PIC fabrication processes. Therefore, we will discuss the advantages and disadvantages of the first two approaches, which can be implemented based on planar PICs.

Out-of-plane generation of optical vortices implies their transmission via free space or optical fiber (using some lens in front of vortex beam emitter in order to have paraxial or focused beam, respectively). Main design solutions for out-of-plane vortex beam emitters include but are not limited to i) VCSEL integrated with micro spiral phase plate [31], ii) annular grating or a set of annularly placed gratings [32]–[36], and iii) ring resonator with azimuthally distributed light-emitting grating [37]–[44]. The last approach has shown robustness, potential for wavelength and OAM tunability, and high purity of the generated OAM states, allowing OAM-multiplexed transmission [40]–[43]. The weak point of this approach is its limited multiplexing scalability, as well as the need of a free space element (lens) to couple the generated beam. Also in this case the generated beams are vector vortex beams, and a quarter-wave plate is needed if we want to transform them into purely phase vortices.

Regarding the in-plane OAM-based solutions, this approach appears advantageous because the vortex beam remains confined within the chip plane, and therefore it can be processed, detected or used in some other way by fabricating more complex (electronic-)photonic integrated circuits. Moreover, in-plane approach allows edge-coupling of the generated vortex modes directly to the fiber or another waveguide without free-space path and the need of any additional optical elements. The weak points of the in-plane approach are its questionable scalability and the need for custom chip fabrication or the use of shorter wavelengths. The latter is caused by the waveguide height of the existing photonic integration platforms, which is usually defined for single-mode operation at telecom wavelengths. However, this raises the questions of compatibility with existing communication systems and availability of laser sources and detectors.

Up to now this approach is much less elaborated and only a few publications on are known [45]–[49]. In [45]–[48], the solutions for generation of OAM beams with azimuthal order of ± 1 have been proposed and numerically modelled. These solutions involve the use of the system of silicon waveguides and directional couplers [45], a waveguide with a single longitudinal trench [46], a hybrid plasmonic waveguide [47], and integrable quarter-wave plates [48]. In [49], authors theoretically investigated propagation and self-imaging of OAM modes in multimode interference waveguides and showed that such devices can be used as OAM mode splitters and couplers. In the papers [52], [53], we have experimentally demonstrated for the first time in-plane propagation of the 1st order quasi-TE vortex modes in a planar rectangular polymer waveguide.

At the same time, to the best of our knowledge, there are no existing works on the problem of optical vortex propagation in rectangular dielectric waveguides for a general case of azimuthal order. Transmission of an ideal vortex mode is known to require a circular cross-section of the waveguide, which inherently provides a propagation with the term $e^{\pm il\varphi}$, defining the phase front helicity (here φ denotes the azimuthal angle). Whereas this condition is met automatically in optical fibers, it is not

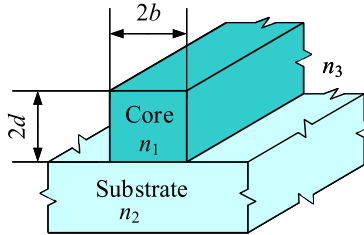


Fig. 1. Waveguide structure under consideration.

obvious in rectangular waveguides, fabricated with the standard lithographical processes. There are works, investigating OAM in the beams, which initially do not have circular symmetry. In particular, in [54] authors have demonstrated that superpositions of free-space Hermite-Gaussian beams can transfer OAM, even though such beams do not explicitly possess the azimuthal phase term. In [55], authors use the Humblet decomposition of the angular momentum to analyze the electromagnetic field in metallic waveguides, and show that the modes carrying OAM and spin can propagate in the metallic waveguides with rectangular cross section. However, for optical waveguides this question in its general statement is still open.

In the current paper, we analyze the possibility of vortex modes transmission over dielectric rectangular waveguides, and consider the problem of waveguide aspect ratio optimization for propagation of such modes. In Section 2, we study the conditions of vortex modes propagation in rectangular optical waveguides using the approximate analytical model based on the Marcatili approach; in Section 3 we show some examples for quasi-TE and quasi-TM modal superpositions for orders $\ell = 1, 2$ and 3 and analyze corresponding OAM spectra; and in Section 4 we discuss the results and make up conclusions.

2. Approximate Analytic Model Based on Marcatili Approach

To verify the possibility of OAM transmission in rectangular dielectric waveguides, let us consider the following superpositions $\mathbf{E}_{\pm\ell}$ of quasi-TE or quasi-TM eigenmodes $\mathbf{E}_{\mu,\nu}$ of a rectangular waveguide:

$$\mathbf{E}_{\pm\ell}(x, y, z) = -i^\ell \sum_{j=0}^{\ell} (\pm i)^j \mathbf{E}_{j, \ell-j}(x, y) e^{-i\beta_{j, \ell-j} z}, \ell = 1, 2, \dots \quad (1)$$

where the eigenmodes $\mathbf{E}_{\mu,\nu}$ are denoted by the spatial indices μ and ν , defining the number of phase changes of the dominant electric field component for π over x and y axes respectively. For each value of the superposition index ℓ , the eigenmodes constituting the superposition (1) are adjacent by their effective refractive indices.

It is known that no strict analytic solution exists for modes of the rectangular waveguides, therefore for the quantitative study of modal fields and corresponding propagation constants below we use a numerical full vector finite difference eigenmode solver in MATLAB [56], [57]. However, to analyze qualitatively the phase front helicity of modal superpositions (1) and approximately calculate the geometrical parameters of the waveguides supporting vortex modes, we can use the approximate analytical method developed by Marcatili [58], [59]. This method is applicable for the modes not close to cutoff, and provides better approximation as the refractive index contrast of the waveguide decreases. Let us consider a typical strip waveguide shown in Fig. 1, where $n_1 > n_2 \geq n_3$. This structure can represent either asymmetric (without cladding) or symmetric (clad) waveguides [59] if we set $n_2 > n_3$ or $n_2 = n_3$ respectively.

According to Marcatili approach, the normalized transverse distribution of dominant electric field component of quasi-TM and quasi-TE eigenmodes with spatial mode indices μ, ν within the core

region can be approximated as:

$$\begin{aligned} \text{Quasi-TM: } E_{\mu,v}^y(x, y) &= \cos \kappa_{\mu}^{x||} (x + b + \eta_{\mu}^{||}) \sin \kappa_{\nu}^{y\perp} (y - d + \xi_{\nu}^{\perp}) = C_{\mu}^{x||}(x) \cdot S_{\nu}^{y\perp}(y), \\ \text{Quasi-TE: } E_{\mu,v}^x(x, y) &= \sin \kappa_{\mu}^{x\perp} (x + b + \eta_{\mu}^{\perp}) \cos \kappa_{\nu}^{y||} (y - d + \xi_{\nu}^{||}) = S_{\mu}^{x\perp}(x) \cdot C_{\nu}^{y||}(y), \end{aligned} \quad (2)$$

where b and d are half-width and half-height of the waveguide respectively; $\kappa_{\mu}^{x||}$, $\kappa_{\mu}^{x\perp}$, and $\kappa_{\nu}^{y||}$, $\kappa_{\nu}^{y\perp}$ are the projections of the wave vector over x and y axes for the slab waveguide eigenmodes with indices μ and ν respectively (here superscripts “||” and “ \perp ” denote respectively the parallel and orthogonal orientations of the mode field polarization relative to the waveguide boundaries, confining the mode over x or y direction). These transverse projections of wave vector satisfy the following eigenvalue equations:

$$\tan 2\kappa^{x||} b = \frac{2\kappa^{x||}\sqrt{(n_1^2 - n_3^2)k_0^2 - (\kappa^{x||})^2}}{2(\kappa^{x||})^2 - (n_1^2 - n_3^2)k_0^2}; \quad (3)$$

$$\tan 2\kappa^{y\perp} d = \frac{n_1^2 \kappa^{y\perp} \left(n_3^2 \sqrt{(n_1^2 - n_2^2)k_0^2 - (\kappa^{y\perp})^2} + n_2^2 \sqrt{(n_1^2 - n_3^2)k_0^2 - (\kappa^{y\perp})^2} \right)}{n_2^2 n_3^2 (\kappa^{y\perp})^2 - n_1^4 \sqrt{((n_1^2 - n_2^2)k_0^2 - (\kappa^{y\perp})^2)((n_1^2 - n_3^2)k_0^2 - (\kappa^{y\perp})^2)}}; \quad (4)$$

$$\tan 2\kappa^{x\perp} b = \frac{2n_1^2 n_3^2 \kappa^{x\perp} \sqrt{(n_1^2 - n_3^2)k_0^2 - (\kappa^{x\perp})^2}}{(n_1^4 + n_3^4)(\kappa^{x\perp})^2 - n_1^4(n_1^2 - n_3^2)k_0^2}; \quad (5)$$

$$\tan 2\kappa^{y||} d = \frac{\kappa^{y||} \left(\sqrt{(n_1^2 - n_2^2)k_0^2 - (\kappa^{y||})^2} + \sqrt{(n_1^2 - n_3^2)k_0^2 - (\kappa^{y||})^2} \right)}{(\kappa^{y||})^2 - \sqrt{((n_1^2 - n_2^2)k_0^2 - (\kappa^{y||})^2)((n_1^2 - n_3^2)k_0^2 - (\kappa^{y||})^2)}}; \quad (6)$$

and the phase parameters η and ξ in (2) can be calculated from the following equations:

$$\begin{aligned} \tan \kappa^{x||} \eta^{||} &= -\frac{1}{\kappa^{x||}} \sqrt{(n_1^2 - n_3^2)k_0^2 - (\kappa^{x||})^2}, \\ \tan \kappa^{y\perp} \xi^{\perp} &= -\frac{n_3^2 \kappa^{y\perp}}{n_1^2 \sqrt{(n_1^2 - n_3^2)k_0^2 - (\kappa^{y\perp})^2}}, \\ \tan \kappa^{x\perp} \eta^{\perp} &= \frac{n_3^2 \kappa^{x\perp}}{n_1^2 \sqrt{(n_1^2 - n_3^2)k_0^2 - (\kappa^{x\perp})^2}}, \\ \tan \kappa^{y||} \xi^{||} &= \frac{1}{\kappa^{y||}} \sqrt{(n_1^2 - n_3^2)k_0^2 - (\kappa^{y||})^2}. \end{aligned} \quad (7)$$

For brevity of further considerations, in equations (2) we introduced the functions $C_{\mu}^{x||}(x)$, $S_{\mu}^{x\perp}(x)$, and $S_{\nu}^{y\perp}(y)$, $C_{\nu}^{y||}(y)$, which define the distributions of the eigenmodes dominant electric field component over the x and y axes, respectively. Then, the dominant electric field component of the modal superposition (1) within the core region in the plane $z = 0$ can be written as:

$$\text{Quasi-TM: } E_{\pm\ell}^y(x, y) = -i^{\ell} \sum_{j=0}^{\ell} (\pm i)^j C_j^{x||}(x) \cdot S_{\ell-j}^{y\perp}(y); \quad (8)$$

$$\text{Quasi-TE: } E_{\pm\ell}^x(x, y) = -i^{\ell} \sum_{j=0}^{\ell} (\pm i)^j S_j^{x\perp}(x) \cdot C_{\ell-j}^{y||}(y). \quad (9)$$

The Taylor series expansion of the functions $C_\mu^{x||}(x)$, $S_\mu^{x\perp}(x)$, $S_\nu^{y\perp}(y)$, $C_\nu^{y||}(y)$ in the vicinity of the waveguide central point ($x = 0$, $y = 0$) gives:

$$C_\mu^{x||}(x) = \sum_{q=0}^{\infty} \frac{(-1)^q}{(2q)!} x^{2q} (\kappa_\mu^{x||})^{2q} \left(\cos \kappa_\mu^{x||} (b + \eta_\mu^{||}) - \frac{x \kappa_\mu^{x||}}{2q+1} \sin \kappa_\mu^{x||} (b + \eta_\mu^{||}) \right); \quad (10)$$

$$S_\nu^{y\perp}(y) = \sum_{q=0}^{\infty} \frac{(-1)^q}{(2q)!} y^{2q} (\kappa_\nu^{y\perp})^{2q} \left(\sin \kappa_\nu^{y\perp} (-d + \xi_\nu^\perp) + \frac{y \kappa_\nu^{y\perp}}{2q+1} \cos \kappa_\nu^{y\perp} (-d + \xi_\nu^\perp) \right); \quad (11)$$

$$S_\mu^{x\perp}(x) = \sum_{q=0}^{\infty} \frac{(-1)^q}{(2q)!} x^{2q} (\kappa_\mu^{x\perp})^{2q} \left(\sin \kappa_\mu^{x\perp} (b + \eta_\mu^\perp) + \frac{x \kappa_\mu^{x\perp}}{2q+1} \cos \kappa_\mu^{x\perp} (b + \eta_\mu^\perp) \right); \quad (12)$$

$$C_\nu^{y||}(y) = \sum_{q=0}^{\infty} \frac{(-1)^q}{(2q)!} y^{2q} (\kappa_\nu^{y||})^{2q} \left(\cos \kappa_\nu^{y||} (-d + \xi_\nu^{||}) - \frac{y \kappa_\nu^{y||}}{2q+1} \sin \kappa_\nu^{y||} (-d + \xi_\nu^{||}) \right). \quad (13)$$

Let us consider the typical practical case when the waveguide cross-section is horizontally symmetric relative to the y axis. Then, obviously, the maximum field amplitude of the even order eigenmodes and the minimum field amplitude of the odd order eigenmodes over the x axis coincide with the point $x = 0$. Therefore, by expressing the sine and cosine terms in (10) and (12) through the functions $C_\mu^{x||}(x)$ and $S_\mu^{x\perp}(x)$ at the point $x = 0$, we can write:

$$\begin{aligned} \cos \kappa_\mu^{x||} (b + \eta_\mu^{||}) &= C_\mu^{x||}(0) = \begin{cases} 1, & \text{even } \mu, \\ 0, & \text{odd } \mu; \end{cases} \\ \sin \kappa_\mu^{x||} (b + \eta_\mu^{||}) &= \sqrt{1 - (C_\mu^{x||}(0))^2} = \begin{cases} 0, & \text{even } \mu, \\ 1, & \text{odd } \mu; \end{cases} \\ \sin \kappa_\mu^{x\perp} (b + \eta_\mu^\perp) &= S_\mu^{x\perp}(0) = \begin{cases} 1, & \text{even } \mu, \\ 0, & \text{odd } \mu; \end{cases} \\ \cos \kappa_\mu^{x\perp} (b + \eta_\mu^\perp) &= \sqrt{1 - (S_\mu^{x\perp}(0))^2} = \begin{cases} 0, & \text{even } \mu, \\ 1, & \text{odd } \mu. \end{cases} \end{aligned} \quad (14)$$

As a next step, we can rewrite (10) and (12) as:

$$C_\mu^{x||}(x) = \begin{cases} \sum_{q=0}^{\infty} \frac{(-1)^q}{(2q)!} x^{2q} (\kappa_\mu^{x||})^{2q}, & \text{even } \mu, \\ \sum_{q=0}^{\infty} \frac{(-1)^{q+1}}{(2q+1)!} x^{2q+1} (\kappa_\mu^{x||})^{2q+1}, & \text{odd } \mu; \end{cases} \quad (15)$$

$$S_\mu^{x\perp}(x) = \begin{cases} \sum_{q=0}^{\infty} \frac{(-1)^q}{(2q)!} x^{2q} (\kappa_\mu^{x\perp})^{2q}, & \text{even } \mu, \\ \sum_{q=0}^{\infty} \frac{(-1)^q}{(2q+1)!} x^{2q+1} (\kappa_\mu^{x\perp})^{2q+1}, & \text{odd } \mu. \end{cases} \quad (16)$$

Moreover, in practical cases, when the eigenmode is propagating not close to cutoff, even though the waveguide is not symmetric relative to x axis, the vertical shift of the maximum amplitude point of the even eigenmode field and the minimum amplitude point of the odd eigenmode field from the waveguide center is much smaller than the waveguide height. Therefore, we can write:

$$\sin \kappa_\nu^{y\perp} (-d + \xi_\nu^\perp) = S_\nu^{y\perp}(0) \rightarrow 0, \text{ odd } \nu; \quad (17)$$

$$\cos \kappa_\nu^{y\perp} (-d + \xi_\nu^\perp) = \sqrt{1 - (S_\nu^{y\perp}(0))^2} \rightarrow 0, \text{ even } \nu; \quad (18)$$

$$\cos \kappa_\nu^{y||} (-d + \xi_\nu^{||}) = C_\nu^{y||}(0) \rightarrow 0, \text{ odd } \nu; \quad (19)$$

$$\sin \kappa_\nu^{y||} (-d + \xi_\nu^{||}) = \sqrt{1 - (C_\nu^{y||}(0))^2} \rightarrow 0, \text{ even } \nu. \quad (20)$$

Let us consider first the simplest case of modal superposition (1) with index $\ell = 1$. For quasi-TM mode, inserting (11) and (15) into (8), we have:

$$\begin{aligned} E_{\pm 1}^y(x, y) = & -i \left(1 + \sum_{q=1}^{\infty} \frac{(-1)^q}{(2q)!} x^{2q} (\kappa_0^{x||})^{2q} \right) \left(\sin \kappa_1^{y\perp} (-d + \xi_1^\perp) + y \kappa_1^{y\perp} \cos \kappa_1^{y\perp} (-d + \xi_1^\perp) \right. \\ & \left. + \sum_{q=1}^{\infty} \frac{(-1)^q}{(2q)!} y^{2q} (\kappa_1^{y\perp})^{2q} \left(\sin \kappa_1^{y\perp} (-d + \xi_1^\perp) + \frac{y \kappa_1^{y\perp}}{2q+1} \cos \kappa_1^{y\perp} (-d + \xi_1^\perp) \right) \right) \\ & \pm \left(-x \kappa_1^{x||} + \sum_{q=1}^{\infty} \frac{(-1)^{q+1}}{(2q+1)!} x^{2q+1} (\kappa_1^{x||})^{2q+1} \right) \left(\sin \kappa_0^{y\perp} (-d + \xi_0^\perp) + y \kappa_0^{y\perp} \cos \kappa_0^{y\perp} (-d + \xi_0^\perp) \right. \\ & \left. + \sum_{q=1}^{\infty} \frac{(-1)^q}{(2q)!} y^{2q} (\kappa_0^{y\perp})^{2q} \left(\sin \kappa_0^{y\perp} (-d + \xi_0^\perp) + \frac{y \kappa_0^{y\perp}}{2q+1} \cos \kappa_0^{y\perp} (-d + \xi_0^\perp) \right) \right), \end{aligned} \quad (21)$$

where zero-order term $-i \sin \kappa_1^{y\perp} (-d + \xi_1^\perp)$ represents the field at the center of waveguide $E_{\pm 1}^y(0, 0)$ and tends to zero due to (17); first-order terms $\mp x \kappa_1^{x||} \sin \kappa_0^{y\perp} (-d + \xi_0^\perp)$ and $-iy \kappa_1^{y\perp} \cos \kappa_1^{y\perp} (-d + \xi_1^\perp)$ under certain condition, considered below, can form an optical vortex of azimuthal order ± 1 ; and the higher order terms contribute to the optical vortices of higher azimuthal orders, carrying higher OAM states. Noteworthy, second-order terms tend to zero because of (17) and (18). And considering the field in the vicinity of waveguide center, the 3rd and higher order terms are much smaller compared to the 1st order terms.

Inserting (13) and (16) into (9), for the quasi-TE mode of $\ell = 1$ we have:

$$\begin{aligned} E_{\pm 1}^x(x, y) = & -i \left(1 + \sum_{q=1}^{\infty} \frac{(-1)^q}{(2q)!} x^{2q} (\kappa_0^{x\perp})^{2q} \right) \left(\cos \kappa_1^{y||} (-d + \xi_1^{||}) - y \kappa_1^{y||} \sin \kappa_1^{y||} (-d + \xi_1^{||}) \right. \\ & \left. + \sum_{q=1}^{\infty} \frac{(-1)^q}{(2q)!} y^{2q} (\kappa_1^{y||})^{2q} \left(\cos \kappa_1^{y||} (-d + \xi_1^{||}) + \frac{y \kappa_1^{y||}}{2q+1} \sin \kappa_1^{y||} (-d + \xi_1^{||}) \right) \right) \\ & \pm \left(x \kappa_1^{x\perp} + \sum_{q=1}^{\infty} \frac{(-1)^q}{(2q+1)!} x^{2q+1} (\kappa_1^{x\perp})^{2q+1} \right) \left(\cos \kappa_0^{y||} (-d + \xi_0^{||}) - y \kappa_0^{y||} \sin \kappa_0^{y||} (-d + \xi_0^{||}) \right. \\ & \left. + \sum_{q=1}^{\infty} \frac{(-1)^q}{(2q)!} y^{2q} (\kappa_0^{y||})^{2q} \left(\cos \kappa_0^{y||} (-d + \xi_0^{||}) + \frac{y \kappa_0^{y||}}{2q+1} \sin \kappa_0^{y||} (-d + \xi_0^{||}) \right) \right). \end{aligned} \quad (22)$$

Similarly to the case of quasi-TM mode, the zero-order term $-i \cos \kappa_1^{y||} (-d + \xi_1^{||})$ represents $E_{\pm 1}^x(0, 0)$ and tends to zero due to (19); first-order terms $\pm x \kappa_1^{x\perp} \cos \kappa_0^{y||} (-d + \xi_0^{||})$ and $iy \kappa_1^{y||} \sin \kappa_1^{y||} (-d + \xi_1^{||})$ can form an optical vortex of azimuthal order ± 1 ; and the higher order terms contribute to the optical vortices of higher azimuthal orders. Second-order terms tend to zero because of (19) and (20), and the third and higher order terms are much smaller compared to the 1st order terms in the vicinity of the waveguide center.

Therefore, in order to optimize the transfer of OAM state ± 1 by quasi-TM and quasi-TE modes of rectangular waveguide, the following conditions should be met:

$$\begin{aligned} \text{Quasi-TM: } & \kappa_1^{x||} \sin \kappa_0^{y\perp} (-d + \xi_0^\perp) = \kappa_1^{y\perp} \cos \kappa_1^{y\perp} (-d + \xi_1^\perp) = A, \\ \text{Quasi-TE: } & \kappa_1^{x\perp} \cos \kappa_0^{y||} (-d + \xi_0^{||}) = \kappa_1^{y||} \sin \kappa_1^{y||} (-d + \xi_1^{||}) = B. \end{aligned} \quad (23)$$

Indeed, taking into account condition (23) and neglecting the 2nd and higher order terms, we have:

$$\begin{aligned} \text{Quasi-TM: } E_{\pm 1}^y(x, y) &= E_{\pm 1}^y(0, 0) \mp A(x \pm iy) = E_{\pm 1}^y(0) \mp A\rho e^{\pm i\varphi}, \\ \text{Quasi-TE: } E_{\pm 1}^x(x, y) &= E_{\pm 1}^x(0, 0) \pm B(x \pm iy) = E_{\pm 1}^x(0) \pm B\rho e^{\pm i\varphi}. \end{aligned} \quad (24)$$

Thus, for the given refractive indices of the waveguide core, substrate and cladding, equations (23) yield a relationship between b and d (waveguide aspect ratio), providing optimized transmission of vortex mode carrying OAM-state ± 1 . It is worth mentioning that condition (23) is different for quasi-TE and quasi-TM modes, i.e., the waveguide geometry cannot be optimized for transfer of vortex modes of both polarizations simultaneously.

Let us assume that the waveguide height d is predefined in order to provide the support of a certain number of eigenmodes. Moreover, the waveguide height is usually fixed by the technological process, and only the waveguide width can be freely changed in order to optimize optical mode propagation. For a given d , we can directly express $\kappa_1^{x||}$ and $\kappa_1^{x\perp}$ from (23) for quasi-TM and quasi-TE modes respectively as:

$$\begin{aligned} \text{Quasi-TM: } \kappa_1^{x||} &= \frac{\kappa_1^{y\perp} \cos \kappa_1^{y\perp} (-d + \xi_1^\perp)}{\sin \kappa_0^{y\perp} (-d + \xi_0^\perp)}, \\ \text{Quasi-TE: } \kappa_1^{x\perp} &= \frac{\kappa_1^{y||} \sin \kappa_1^{y||} (-d + \xi_1^{||})}{\cos \kappa_0^{y||} (-d + \xi_0^{||})}. \end{aligned} \quad (25)$$

Hence, b should satisfy the eigenvalue equations (3) and (5) for $\kappa_1^{x||}$ and $\kappa_1^{x\perp}$ respectively:

$$\begin{aligned} \text{Quasi-TM: } b &= \frac{1}{2\kappa_1^{x||}} \left(\arctan \frac{2\kappa_1^{x||} \sqrt{(n_1^2 - n_3^2) k_0^2 - (\kappa_1^{x||})^2}}{2(\kappa_1^{x||})^2 - (n_1^2 - n_3^2) k_0^2} + K\pi \right), \\ \text{Quasi-TE: } b &= \frac{1}{2\kappa_1^{x\perp}} \left(\arctan \frac{2n_1^2 n_3^2 \kappa_1^{x\perp} \sqrt{(n_1^2 - n_3^2) k_0^2 - (\kappa_1^{x\perp})^2}}{(n_1^4 + n_3^4)(\kappa_1^{x\perp})^2 - n_1^4(n_1^2 - n_3^2) k_0^2} + K\pi \right), \end{aligned} \quad (26)$$

where K is an integer, whose value can be determined from the requirement for b to be physically meaningful (it should be a positive number closest to the value of d , to have the waveguide aspect ratio not far from 1). For the cases of waveguides that we tested, K was most often equal to 2, and sometimes equal to 1.

At the same time, propagation constants $\beta = 2\pi n_{\text{eff}}/\lambda$ of the eigenmodes constituting the sum (1) should be matched in order to provide a constant helical phase front of the propagating vortex mode. Thus, for the case $\ell = 1$, we should have $\beta_{01} = \beta_{10}$, that is:

$$\begin{aligned} \text{Quasi-TM: } (\kappa_0^{x||})^2 + (\kappa_1^{y\perp})^2 &= (\kappa_1^{x||})^2 + (\kappa_0^{y\perp})^2, \\ \text{Quasi-TE: } (\kappa_0^{x\perp})^2 + (\kappa_1^{y||})^2 &= (\kappa_1^{x\perp})^2 + (\kappa_0^{y||})^2. \end{aligned} \quad (27)$$

Therefore, equations (27) provide another one condition, which apparently does not coincide with the condition (26). The corresponding values of β (or n_{eff}), providing phase matching between the constituent eigenmodes \mathbf{E}_{01} and \mathbf{E}_{10} , can be accurately found using numerical modeling.

Now let us consider the possibility of propagation of the vortex mode with 2nd azimuthal order in the rectangular waveguide. Equations (2) for $\ell = 2$, after inserting (11), (13), (14), look as follows:

$$\begin{aligned}
 & \text{Quasi-TM: } E_{\pm 2}^y(x, y) \\
 &= \left(1 - \frac{1}{2}x^2(\kappa_0^{x||})^2 + \sum_{q=2}^{\infty} \frac{(-1)^q}{(2q)!} x^{2q} (\kappa_0^{x||})^{2q} \right) \left(\sin \kappa_2^{y\perp}(-d + \xi_2^\perp) + y \kappa_2^{y\perp} \cos \kappa_2^{y\perp}(-d + \xi_2^\perp) \right. \\
 &\quad \left. - \frac{1}{2}y^2(\kappa_2^{y\perp})^2 \sin \kappa_2^{y\perp}(-d + \xi_2^\perp) - \frac{1}{6}y^3(\kappa_2^{y\perp})^3 \cos \kappa_2^{y\perp}(-d + \xi_2^\perp) + \tilde{S}_2^{y\perp}(y) \right) \\
 &\pm i \left(-x \kappa_1^{x||} + \frac{1}{6}x^3(\kappa_1^{x||})^3 + \sum_{q=2}^{\infty} \frac{(-1)^{q+1}}{(2q+1)!} x^{2q+1} (\kappa_1^{x||})^{2q+1} \right) \left(\sin \kappa_1^{y\perp}(-d + \xi_1^\perp) \right. \\
 &\quad \left. + y \kappa_1^{y\perp} \cos \kappa_1^{y\perp}(-d + \xi_1^\perp) - \frac{1}{2}y^2(\kappa_1^{y\perp})^2 \sin \kappa_1^{y\perp}(-d + \xi_1^\perp) \right. \\
 &\quad \left. - \frac{1}{6}y^3(\kappa_1^{y\perp})^3 \cos \kappa_1^{y\perp}(-d + \xi_1^\perp) + \tilde{S}_1^{y\perp}(y) \right) - \left(1 - \frac{1}{2}x^2(\kappa_2^{x||})^2 + \sum_{q=2}^{\infty} \frac{(-1)^q}{(2q)!} x^{2q} (\kappa_2^{x||})^{2q} \right) \\
 &\times \left(\sin \kappa_0^{y\perp}(-d + \xi_0^\perp) + y \kappa_0^{y\perp} \cos \kappa_0^{y\perp}(-d + \xi_0^\perp) \right. \\
 &\quad \left. - \frac{1}{2}y^2(\kappa_0^{y\perp})^2 \sin \kappa_0^{y\perp}(-d + \xi_0^\perp) - \frac{1}{6}y^3(\kappa_0^{y\perp})^3 \cos \kappa_0^{y\perp}(-d + \xi_0^\perp) + \tilde{S}_0^{y\perp}(y) \right), \tag{28}
 \end{aligned}$$

where $\tilde{S}_v^{y\perp}(y) = \sum_{q=2}^{\infty} \frac{(-1)^q}{(2q)!} y^{2q} (\kappa_v^{y\perp})^{2q} (\sin \kappa_v^{y\perp}(-d + \xi_v^\perp) + \frac{y \kappa_v^{y\perp}}{2q+1} \cos \kappa_v^{y\perp}(-d + \xi_v^\perp))$.

Quasi-TE: $E_{\pm 2}^x(x, y)$

$$\begin{aligned}
 &= \left(1 - \frac{1}{2}x^2(\kappa_0^{x\perp})^2 + \sum_{q=2}^{\infty} \frac{(-1)^q}{(2q)!} x^{2q} (\kappa_0^{x\perp})^{2q} \right) \left(\cos \kappa_2^{y||}(-d + \xi_2^{||}) - y \kappa_2^{y||} \sin \kappa_2^{y||}(-d + \xi_2^{||}) \right. \\
 &\quad \left. - \frac{1}{2}y^2(\kappa_2^{y||})^2 \cos \kappa_2^{y||}(-d + \xi_2^{||}) + \frac{1}{6}y^3(\kappa_2^{y||})^3 \sin \kappa_2^{y||}(-d + \xi_2^{||}) + \tilde{C}_2^{y||}(y) \right) \\
 &\pm i \left(x \kappa_2^{x\perp} - \frac{1}{6}x^3(\kappa_1^{x\perp})^3 + \sum_{q=2}^{\infty} \frac{(-1)^{q+1}}{(2q+1)!} x^{2q+1} (\kappa_1^{x\perp})^{2q+1} \right) \left(\cos \kappa_1^{y||}(-d + \xi_1^{||}) - y \kappa_1^{y||} \sin \kappa_1^{y||}(-d + \xi_1^{||}) \right. \\
 &\quad \left. - \frac{1}{2}y^2(\kappa_1^{y||})^2 \cos \kappa_1^{y||}(-d + \xi_1^{||}) + \frac{1}{6}y^3(\kappa_1^{y||})^3 \sin \kappa_1^{y||}(-d + \xi_1^{||}) + \tilde{C}_1^{y||}(y) \right) \\
 &\quad - \left(1 - \frac{1}{2}x^2(\kappa_2^{x\perp})^2 + \sum_{q=2}^{\infty} \frac{(-1)^q}{(2q)!} x^{2q} (\kappa_2^{x\perp})^{2q} \right) \left(\cos \kappa_0^{y||}(-d + \xi_0^{||}) - y \kappa_0^{y||} \sin \kappa_0^{y||}(-d + \xi_0^{||}) \right) \\
 &\quad - \frac{1}{2}y^2(\kappa_0^{y||})^2 \cos \kappa_0^{y||}(-d + \xi_0^{||}) + \frac{1}{6}y^3(\kappa_0^{y||})^3 \sin \kappa_0^{y||}(-d + \xi_0^{||}) + \tilde{C}_0^{y||}(y), \tag{29}
 \end{aligned}$$

where $\tilde{C}_v^{y||}(y) = \sum_{q=2}^{\infty} \frac{(-1)^q}{(2q)!} y^{2q} (\kappa_v^{y||})^{2q} (\cos \kappa_v^{y||}(-d + \xi_v^{||}) - \frac{y \kappa_v^{y||}}{2q+1} \sin \kappa_v^{y||}(-d + \xi_v^{||}))$.

Zero-order terms $\sin \kappa_2^{y\perp}(-d + \xi_2^\perp) - \sin \kappa_0^{y\perp}(-d + \xi_0^\perp)$ in (28), and $\cos \kappa_2^{y||}(-d + \xi_2^{||}) - \cos \kappa_0^{y||}(-d + \xi_0^{||})$ in (29), represent the fields $E_{\pm 2}^y(0, 0)$ and $E_{\pm 2}^x(0, 0)$ at the center of waveguide respectively, and are relatively small, because the minuend and the subtrahend are both close to the maximum value of normalized electric field, i.e., one. First-order terms $y \kappa_2^{y\perp} \cos \kappa_2^{y\perp}(-d + \xi_2^\perp)$,

$\mp x\kappa_1^{x||}\sin\kappa_1^{y\perp}(-d+\xi_1^\perp)$ and $y\kappa_0^{y\perp}\cos\kappa_0^{y\perp}(-d+\xi_0^\perp)$ in (28), and $-y\kappa_2^{y||}\sin\kappa_2^{y||}(-d+\xi_2^{||})$, $\pm ix\kappa_1^{x\perp}\cos\kappa_1^{y||}(-d+\xi_1^{||})$ and $y\kappa_0^{y||}\sin\kappa_0^{y||}(-d+\xi_0^{||})$ in (29), contributing to the 1st order vortex mode, tend to 0 because of (17)–(20). A similar conclusion can be drawn for the 3rd order terms.

Second order terms could form an optical vortex with the azimuthal order ± 2 , if the following conditions hold:

$$\begin{aligned} \text{Quasi-TM: } & (\kappa_0^{x||})^2 \sin\kappa_2^{y\perp}(-d+\xi_2^\perp) - (\kappa_2^{x||})^2 \sin\kappa_0^{y\perp}(-d+\xi_0^\perp) \\ & = (\kappa_0^{y\perp})^2 \sin\kappa_0^{y\perp}(-d+\xi_0^\perp) - (\kappa_2^{y\perp})^2 \sin\kappa_2^{y\perp}(-d+\xi_2^\perp) = \kappa_1^{x||}\kappa_1^{y\perp}\cos\kappa_1^{y\perp}(-d+\xi_1^\perp) = A, \\ \text{Quasi-TE: } & (\kappa_0^{x\perp})^2 \cos\kappa_2^{y||}(-d+\xi_2^{||}) - (\kappa_2^{x\perp})^2 \cos\kappa_0^{y||}(-d+\xi_0^{||}) \\ & = (\kappa_0^{y||})^2 \cos\kappa_0^{y||}(-d+\xi_0^{||}) - (\kappa_2^{y||})^2 \cos\kappa_2^{y||}(-d+\xi_2^{||}) = \kappa_1^{x\perp}\kappa_1^{y||}\sin\kappa_1^{y||}(-d+\xi_1^{||}) = B. \end{aligned} \quad (30)$$

In this case, if we neglect the 1st, 3rd and higher order terms in the vicinity of waveguide center, we will have there:

$$\begin{aligned} \text{Quasi-TM: } E_{\pm 2}^y(x, y) &= E_{\pm 2}^y(0, 0) + \frac{1}{2}A(x^2 - y^2 \pm i2xy) = E_{\pm 2}^y(0) + \frac{1}{2}A\rho^2(\cos 2\varphi \pm i\sin 2\varphi) \\ &= E_{\pm 2}^y(0) + \frac{1}{2}A\rho^2 e^{\pm i2\varphi}, \\ \text{Quasi-TE: } E_{\pm 2}^x(x, y) &= E_{\pm 2}^x(0, 0) + \frac{1}{2}B(x^2 - y^2 \pm i2xy) = E_{\pm 2}^x(0) + \frac{1}{2}B\rho^2(\cos 2\varphi \pm i\sin 2\varphi) \\ &= E_{\pm 2}^x(0) + \frac{1}{2}B\rho^2 e^{\pm i2\varphi}. \end{aligned} \quad (31)$$

In order to comply with the phase matching condition between the eigenmodes constituting the sum (1) in case of the vortex mode of 2nd azimuthal order, the equality $\beta_{11} = \beta_{02} = \beta_{20}$ should be met, or:

$$\begin{aligned} \text{Quasi-TM: } & (\kappa_1^{x||})^2 + (\kappa_1^{y\perp})^2 = (\kappa_0^{x||})^2 + (\kappa_2^{y\perp})^2 = (\kappa_2^{x||})^2 + (\kappa_0^{y\perp})^2, \\ \text{Quasi-TE: } & (\kappa_1^{x\perp})^2 + (\kappa_1^{y||})^2 = (\kappa_0^{x\perp})^2 + (\kappa_2^{y||})^2 = (\kappa_2^{x\perp})^2 + (\kappa_0^{y||})^2. \end{aligned} \quad (32)$$

Unfortunately, in typical dielectric waveguides, manufactured in standard PIC processes, neither condition (30), nor condition (32) can be met (only two of three terms in these equalities can be equal). Thus, we can optimize the waveguide geometry only in such a way that two constituent eigenmodes (the eigenmodes with indices 02 and 20) propagate with the same effective index, but the third mode (the eigenmode with indices 11) propagates with its own effective index. Therefore, the optical vortex of 2nd azimuthal order will exist in certain planes separated from each other over z axis by the beat length $\Lambda = 2\pi/\Delta\beta$, where $\Delta\beta$ is the difference between the propagation constants β_{11} and $\beta_{02} = \beta_{20}$.

By analogy with the cases $\ell = 1$ and 2, superposition (1) can be rewritten for any order ℓ . However, the problem of waveguide geometry optimization regarding the OAM state purity and phase matching conditions becomes increasingly more complex for higher azimuthal orders, as more eigenmodes become involved.

3. Results of Numerical Modeling

As an example for numerical modeling, we consider in the following silicon nitride waveguides ($n_1 = 1.9963$ at $\lambda = 1550$ nm), deposited on pure silica substrate ($n_2 = 1.444$ at $\lambda = 1550$ nm). We investigated the waveguide in both symmetric and asymmetric configurations, i.e., with and without SiO_2 cladding, respectively. All calculations are made at the wavelength $\lambda = 1550$ nm. Eigenmode fields and effective indices have been calculated in MATLAB using the full-vector finite difference

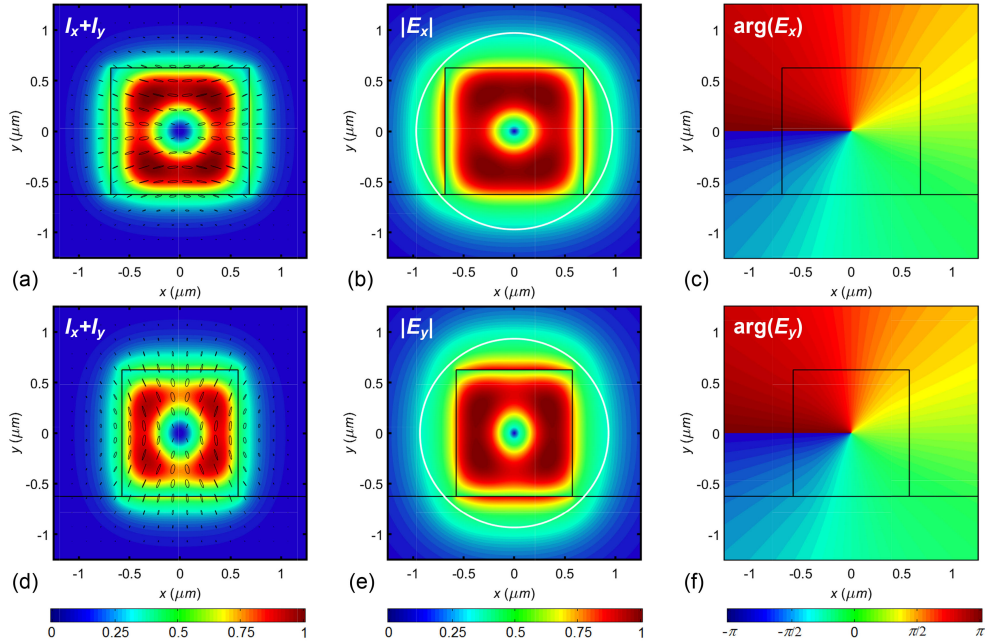


Fig. 2. Numerical calculation results for the normalized intensity distribution of transversal field components superimposed with polarization map (a–d), normalized absolute amplitude distribution of dominant electric field component (b, e) and phase distribution of dominant electric field component (c, f) of the quasi-TE (a–c) and quasi-TM (d–f) quasi-degenerate modes of order $\ell = 1$ in the symmetric (silica clad) silicon nitride waveguides optimized for phase-matched propagation of the constituent eigenmodes ($\beta_{01} \approx \beta_{10}$). White circumferences on the amplitude distributions (b) and (e) show the area considered for OAM spectrum calculation.

modesolver for dielectric waveguides, available at [56] and described in [57]. In order to combine the eigenmodes according to (1) and analyze the OAM spectra of the resulting superpositions, we have implemented a specific code in MATLAB.

In order to investigate propagation of quasi-degenerate mode of order $\ell = 1$, we set the core height to 1250 nm ($d = 625$ nm), which guarantees the support of quasi-TE and quasi-TM eigenmodes with indices $v = 0$ and 1 over vertical y axis, but not the modes of higher vertical indices. Then, in order to provide condition (23), the waveguide width, calculated according to (26) and rounded to the nearest 1 nm, will have the values 1405 nm and 1101 nm for quasi-TE and quasi-TM modes, respectively, for the symmetric waveguide, and 1520 nm and 1145 nm, respectively, for the asymmetric waveguide. In order to provide phase matching between the modes with indices 01 and 10, constituting the quasi-degenerate mode of order $\ell = 1$, the waveguide width (rounded to the nearest 1 nm) for quasi-TE and quasi-TM modes should have the values 1370 nm and 1149 nm, respectively, for the symmetric waveguide, and 1502 nm and 1163 nm, respectively, for the asymmetric waveguide without cladding.

Therefore, the waveguide widths calculated for each mode type according to the condition (23) and the condition $\beta_{01} \approx \beta_{10}$ differ, but the difference is not large: for the symmetric waveguide it is about –2.5% and 4.4% for quasi-TE and quasi-TM modes, respectively, and for asymmetric case it is only about –1.2% and 1.6% for quasi-TE and quasi-TM modes, respectively.

We expanded the dominant electric field component over angular harmonics in order to estimate the OAM distribution of the calculated quasi-degenerate modes [60]. For the calculations, we take the circular area, which is centered at the central singularity point of the mode and confined by the radius at which the amplitude of dominant field component falls to $1/e$ of its maximum value (see the middle column of Figures 2–5). The resulting normalized powers of OAM states for the quasi-degenerate mode of order $\ell = 1$ are summarized in Tables 1 and 2 for the symmetric and

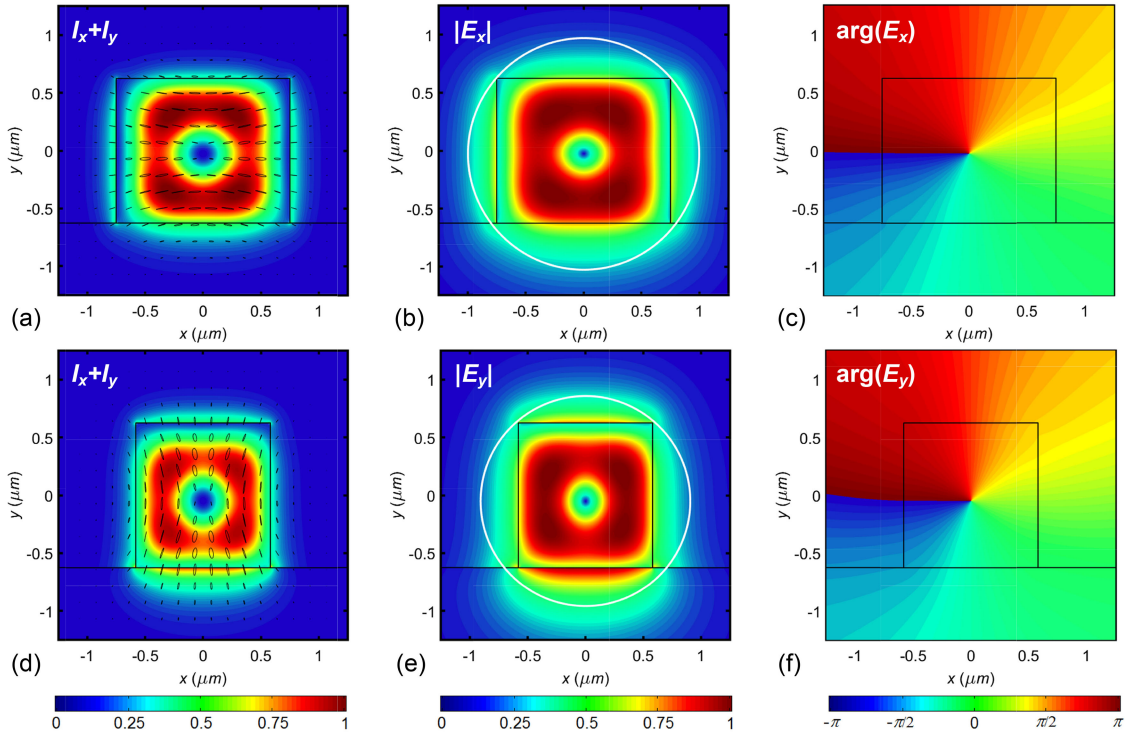


Fig. 3. Numerical calculation results for the normalized intensity distribution of transversal field components superimposed with polarization map (a, d), normalized absolute amplitude distribution of dominant electric field component (b, e) and phase distribution of dominant electric field component (c, f) of the quasi-TE (a–c) and quasi-TM (d–f) quasi-degenerate modes of order $\ell = 1$ in the asymmetric silicon nitride waveguides (without cladding) optimized for phase-matched propagation of the constituent eigenmodes ($\beta_{01} \approx \beta_{10}$). White circumferences on the amplitude distributions (b) and (e) show the area considered for OAM spectrum calculation.

asymmetric waveguides, respectively. For brevity, we show here the values for the target OAM state $+1$ and four next highest values, corresponding to the OAM states -1 , $+3$, -3 , and $+5$. For the quasi-degenerate mode of opposite order $-\ell$, the OAM spectra are similar, but mirrored around zero OAM state.

As we can see from Tables 1 and 2, for each optimized waveguide the dominant field component of quasi-degenerate mode with $\ell = 1$ indeed carries the OAM state $+1$ with high purity, slightly lower than 1 (and the same holds for the quasi-degenerate mode with inverse helicity, which carries OAM state -1). The next highest OAM states contained in the dominant field component are the several odd OAM states near to the target one. This is consistent with the theoretical predictions, made in Section 2. Noteworthy, in the case of waveguide width optimized according to the condition $\beta_{01} \approx \beta_{10}$, the purity of the target OAM state is slightly higher than in the case when waveguide width was calculated from (26), which can be explained by the approximate nature of the Marcatili approach. Therefore, it can provide a qualitative analysis of the mode field characteristics, but for more precise quantitative analysis, especially in high index contrast waveguides, a numerical calculation is preferred.

Figures 2 and 3 show the field profiles of the quasi-degenerate mode for $\ell = 1$ for the symmetric and asymmetric silicon nitride waveguides, when the waveguide width is optimized for phase-matched propagation of the constituent eigenmodes (for the quasi-degenerate mode of order $-\ell$, the mode fields are similar, but the phase profiles of dominant electric field component have an

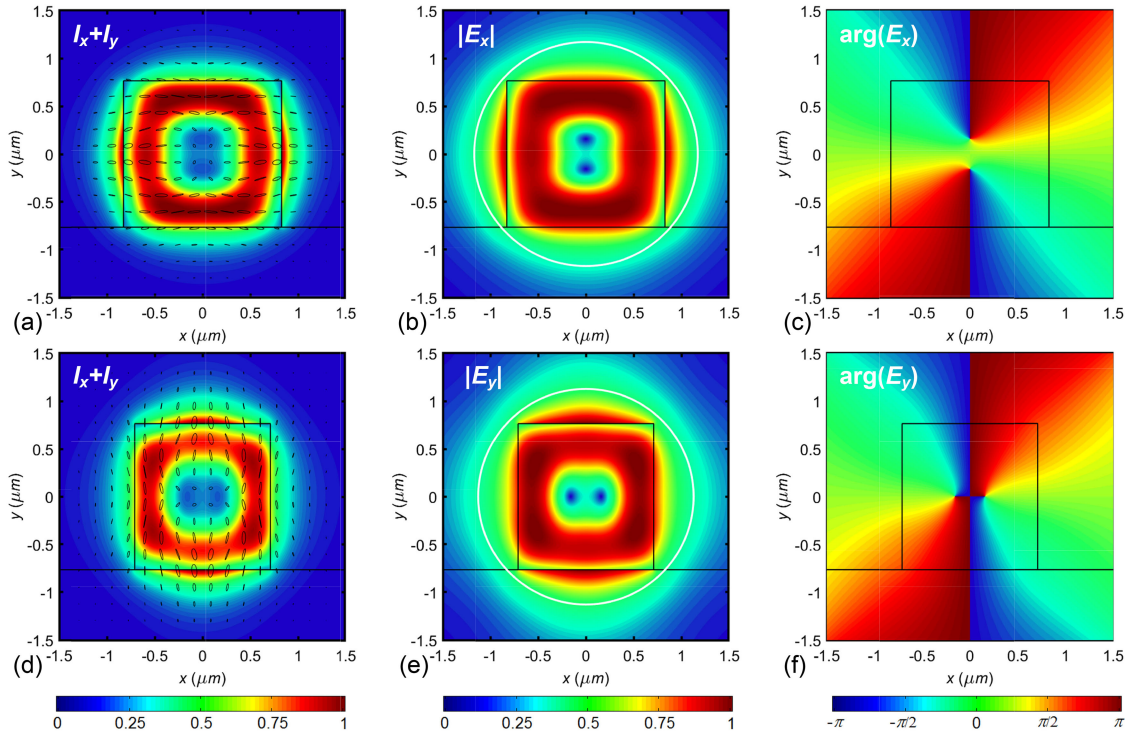


Fig. 4. Numerical calculation results for the normalized intensity distribution of transversal field components superimposed with polarization map (a, d), normalized absolute amplitude distribution of dominant electric field component (b, e) and phase distribution of dominant electric field component (c, f) for the superpositions of quasi-TE (a–c) and quasi-TM (d–f) modes of order $\ell = 2$ in the symmetric silicon nitride waveguides of height 1530 nm at $z = 0$. White circumferences on the amplitude distributions (b) and (e) show the area considered for OAM spectrum calculation.

inverse direction of helicity). For the waveguides with the width calculated to satisfy condition (23), the field profiles visually look very similar, so for the sake of brevity they are not shown.

From Table 1 the observation can be made, that in the symmetric waveguide higher OAM purity can be achieved, which can be intuitively explained by the symmetric field distribution in that case, and vertical asymmetry of the field when the substrate and cladding have different refractive indices.

For the case $\ell = 2$, let us consider the symmetric silicon nitride waveguide with a height of 1530 nm ($d = 765$ nm), which provides propagation of the quasi-TE and quasi-TM eigenmodes with indices ν up to 2, but the higher order eigenmodes are beyond the cutoff. As the numerical calculations show, when the waveguide aspect ratio is close to 1, the eigenmodes of the same polarization with indices 02 and 20 couple with each other. As a result, there are two new aggregate modes with the field distributions corresponding respectively to the sum and difference (with some coefficients) of the theoretical eigenmodes \mathbf{E}_{02} and \mathbf{E}_{20} . Therefore, we can directly use the aggregate mode with the field distribution $(\mathbf{E}_{02} - \mathbf{E}_{20})$, together with the eigenmode \mathbf{E}_{11} , to combine superposition (1) for $\ell = 2$. We set the waveguide width in such a way, that the coupled theoretical eigenmodes \mathbf{E}_{02} and \mathbf{E}_{20} have equal shares in the aggregate sum and difference modes (this can be determined from the phase distributions when subtracting or summing back the aggregate modes). Thus, for the given waveguide height, its width should be 1656 and 1420 nm for the quasi-TE and quasi-TM modes, respectively. Figure 4 shows the field distributions of the modal superpositions (1) for $\ell = 2$ in the plain $z = 0$, and the Table 3 summarizes the corresponding OAM spectra, effective indices of the constituent eigenmodes and the beat lengths. Even though the singularity point at the waveguide center is divided into two separate singularities of topological

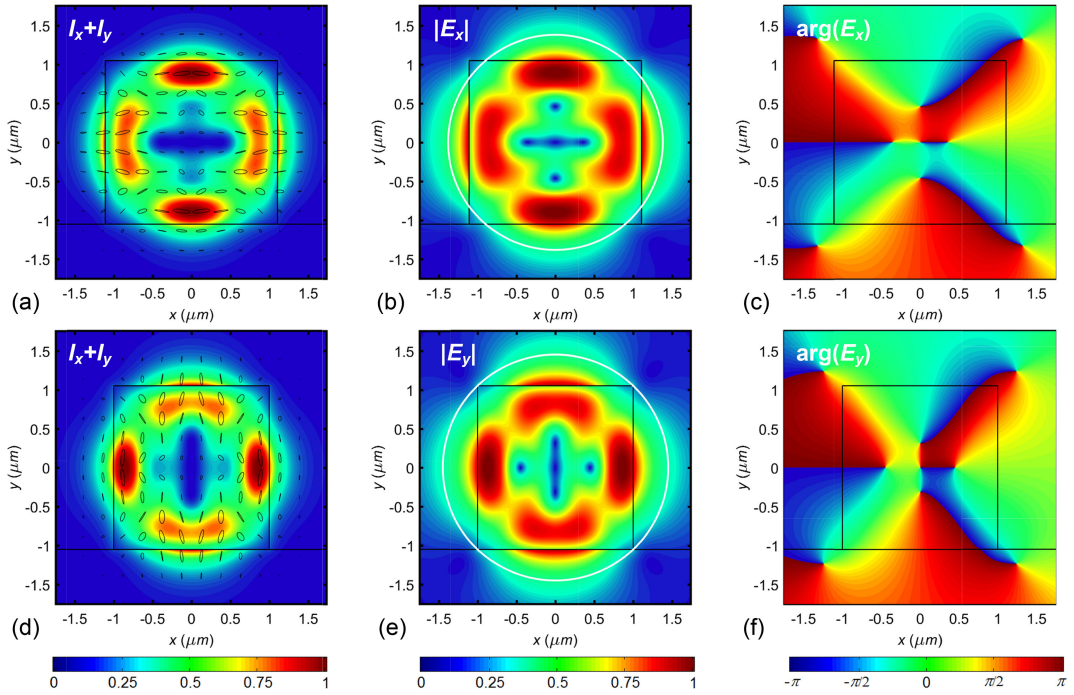


Fig. 5. Numerical calculation results for the normalized intensity distribution of transversal field components superimposed with polarization map (a, d), normalized absolute amplitude distribution of dominant electric field component (b, e) and phase distribution of dominant electric field component (c, f) for the superpositions of quasi-TE (a–c) and quasi-TM (d–f) modes of order $\ell = 3$ in the symmetric silicon nitride waveguides of height 2100 nm at $z = 0$. White circumferences on the amplitude distributions (b) and (e) show the area considered for OAM spectrum calculation.

TABLE 1
Parameters of the Quasi-Degenerate Mode of Order $\ell = 1$ in the Symmetric Waveguide of Height $2d = 1250$ nm

Waveguide optimization condition	Waveguide width ($2b$), nm	$n_{\text{eff}\,10}$	$n_{\text{eff}\,01}$	$ \Delta n_{\text{eff}} $	Normalized power of OAM states in the dominant electric field component				
					+1	-1	+3	-3	+5
Quasi-TE, condition (23)	1405	1.69810	1.69222	$5.877 \cdot 10^{-3}$	0.99660	$6.51 \cdot 10^{-4}$	$5.80 \cdot 10^{-4}$	$8.62 \cdot 10^{-4}$	$9.00 \cdot 10^{-4}$
Quasi-TE, $\beta_{01} \approx \beta_{10}$	1370	1.68871	1.68868	$2.891 \cdot 10^{-5}$	0.99688	$4.20 \cdot 10^{-4}$	$3.76 \cdot 10^{-4}$	$9.13 \cdot 10^{-4}$	$9.46 \cdot 10^{-4}$
Quasi-TM, condition (23)	1101	1.62668	1.63754	$1.087 \cdot 10^{-2}$	0.99611	$1.03 \cdot 10^{-3}$	$9.14 \cdot 10^{-4}$	$7.67 \cdot 10^{-4}$	$8.16 \cdot 10^{-4}$
Quasi-TM, $\beta_{01} \approx \beta_{10}$	1149	1.64321	1.64329	$7.370 \cdot 10^{-5}$	0.99665	$5.19 \cdot 10^{-4}$	$4.66 \cdot 10^{-4}$	$9.09 \cdot 10^{-4}$	$9.43 \cdot 10^{-4}$

charge 1, the calculation over the analyzed cross-section at $z = 0$ shows the normalized power of the OAM state +2 in the dominant field component not far from 1. As expected from the analytical model, the next highest OAM components contained in the dominant field projection are the several even states near to the OAM state +2 (see Table 3).

The difference Δn_{eff} between effective indices of the eigenmode \mathbf{E}_{11} and the aggregate mode ($\mathbf{E}_{02} - \mathbf{E}_{20}$) decreases farther from cutoff. For example, if we change the waveguide height to 1800 nm, then Δn_{eff} becomes lower than in the case of the 1530 nm height waveguide, and correspondingly the beat length Λ becomes larger (see Table 3). At the same time, the normalized power of the target OAM state +2 becomes slightly higher.

Let us also consider a modal superposition (1) for the case $\ell = 3$. For that, we set the waveguide height to 2100 nm ($d = 1050$ nm), which provides propagation of the eigenmodes \mathbf{E}_{12} , \mathbf{E}_{21} , \mathbf{E}_{30} and \mathbf{E}_{03} , needed to combine the superposition. The waveguide widths for quasi-TE and quasi-TM modes are chosen at the cross point of the effective index curves for the eigenmodes \mathbf{E}_{30} and \mathbf{E}_{03} , and rounded to 1 nm. At this point, the effective index difference between the eigenmodes \mathbf{E}_{12}

TABLE 2

Parameters of the Quasi-Degenerate Mode of Order $\ell = 1$ in the Asymmetric Waveguide of Height $2d = 1250$ nm

Waveguide optimization condition	Waveguide width ($2b$), nm	$n_{eff\ 10}$	$n_{eff\ 01}$	$ \Delta n_{eff} $	Normalized power of OAM states in the dominant electric field component				
					+1	-1	+3	-3	+5
Quasi-TE, condition (23)	1520	1.67951	1.67539	$4.126 \cdot 10^{-3}$	0.99482	$9.60 \cdot 10^{-4}$	$8.16 \cdot 10^{-4}$	$1.30 \cdot 10^{-3}$	$1.36 \cdot 10^{-3}$
Quasi-TE, $\beta_{01} \approx \beta_{10}$	1502	1.67365	1.67358	$6.688 \cdot 10^{-5}$	0.99504	$8.24 \cdot 10^{-4}$	$7.05 \cdot 10^{-4}$	$1.32 \cdot 10^{-3}$	$1.37 \cdot 10^{-3}$
Quasi-TM, condition (23)	1145	1.58810	1.59367	$5.575 \cdot 10^{-3}$	0.99527	$6.55 \cdot 10^{-4}$	$5.84 \cdot 10^{-4}$	$1.12 \cdot 10^{-3}$	$1.18 \cdot 10^{-3}$
Quasi-TM, $\beta_{01} \approx \beta_{10}$	1163	1.59592	1.59593	$5.139 \cdot 10^{-6}$	0.99563	$3.85 \cdot 10^{-4}$	$3.55 \cdot 10^{-4}$	$1.16 \cdot 10^{-3}$	$1.21 \cdot 10^{-3}$

TABLE 3

Parameters of the Modal Superpositions for the Order $\ell = 2$ in the Symmetric Waveguide

Mode type	Waveguide height ($2d$), nm	Waveguide width ($2b$), nm	$n_{eff\ 11}$	$n_{eff\ 02-20}$	$ \Delta n_{eff} $	$\Lambda, \mu m$	Normalized power of OAM states in the dominant electric field component at $z = 0$				
							+2	+4	+8	-4	-2
Quasi-TE	1530	1656	1.63606	1.54676	0.08930	17.358	0.96057	$4.86 \cdot 10^{-4}$	$1.77 \cdot 10^{-4}$	$2.09 \cdot 10^{-4}$	$5.41 \cdot 10^{-5}$
Quasi-TM	1530	1420	1.58708	1.48951	0.09757	15.886	0.95799	$5.72 \cdot 10^{-4}$	$2.43 \cdot 10^{-4}$	$2.68 \cdot 10^{-4}$	$2.92 \cdot 10^{-5}$
Quasi-TE	1800	1944	1.72396	1.65477	0.06918	22.404	0.97420	$1.27 \cdot 10^{-4}$	$6.48 \cdot 10^{-5}$	$8.72 \cdot 10^{-5}$	$3.46 \cdot 10^{-5}$
Quasi-TM	1800	1664	1.68415	1.60542	0.07874	19.686	0.97097	$1.50 \cdot 10^{-4}$	$9.89 \cdot 10^{-5}$	$1.25 \cdot 10^{-4}$	$5.56 \cdot 10^{-5}$

TABLE 4

Propagation Parameters of the Modal Superpositions for the Order $\ell = 3$ in the Symmetric Waveguide of Height $2d = 2100$ nm

Mode type	Waveguide width ($2b$), nm	$n_{eff\ 21}$	$n_{eff\ 12}$	$n_{eff\ 30}$	$n_{eff\ 03}$	$ \Delta n_{eff\ 21-12} $	$ \Delta n_{eff\ 30-03} $	$ \Delta n_{eff\ max} $	$\Lambda_{min}, \mu m$
Quasi-TE	2216	1.64984	1.64220	1.54771	1.54757	$7.643 \cdot 10^{-3}$	$1.388 \cdot 10^{-4}$	0.10227	15.156
Quasi-TM	2000	1.60740	1.61698	1.50984	1.50988	$9.581 \cdot 10^{-3}$	$3.983 \cdot 10^{-5}$	0.10714	14.467

TABLE 5

Main OAM Components of the Modal Superpositions for the Order $\ell = 3$ in the Symmetric Waveguide of Height $2d = 2100$ nm

Mode type	Waveguide width ($2b$), nm	Normalized power of OAM states in the dominant electric field component at $z = 0$					
		+3	+5	+7	+11	-1	-5
Quasi-TE	2216	0.78865	$2.32 \cdot 10^{-3}$	$9.73 \cdot 10^{-3}$	$2.90 \cdot 10^{-3}$	$1.18 \cdot 10^{-3}$	$1.73 \cdot 10^{-3}$
Quasi-TM	2000	0.79597	$3.43 \cdot 10^{-3}$	$1.47 \cdot 10^{-2}$	$3.51 \cdot 10^{-3}$	$6.50 \cdot 10^{-3}$	$1.34 \cdot 10^{-3}$

and \mathbf{E}_{21} is also not large (see Table 4). So the values of the minimum beat length Λ_{min} , shown in Table 4, will be defined by the eigenmodes \mathbf{E}_{21} and \mathbf{E}_{03} for the quasi-TE superposition, and the eigenmodes \mathbf{E}_{12} and \mathbf{E}_{30} for the quasi-TM superposition.

Figure 5 shows the field distributions of the quasi-TE and quasi-TM modal superpositions of order $\ell = 3$ in the plain $z = 0$, and Table 5 shows the corresponding OAM distributions in the dominant field component for the target OAM state +3 and several other highest OAM components.

As can be seen from the right column of Figure 5, the dominant field component possesses a helical phase distribution with azimuthal order +3, and this OAM component dominates in the OAM spectrum. However, the singularity point at the waveguide center is divided into five separate singularities of first order, and as a result, the normalized power of OAM state +3 is substantially lower than 1 (0.78865 for quasi-TE superposition, and 0.79597 for quasi-TM superposition).

4. Discussion and Conclusions

We have theoretically demonstrated the possibility of vortex mode transmission over few-mode dielectric rectangular waveguides based on the results of approximate analytic modeling, verified and refined by the numerical simulation results.

It has been shown, that for the vortex modes of 1st order, the waveguide geometry can be optimized to provide phase matched propagation of the two constituent eigenmodes, and the resulting quasi-degenerate quasi-TE or quasi-TM mode will have the purity of target OAM state close to 100%. Therefore, the vortex mode of azimuthal order ± 1 , once coupled to or generated in a planar waveguide, should propagate with the helical phase front over the distances relevant to the chip scale. It is worth mentioning, that the waveguide geometry should be specifically optimized for transmission of either quasi-TE or quasi-TM optical vortex mode. Regarding the OAM states purity, the symmetric waveguide structure is preferred.

The modal superpositions of order $\ell = 2$ and higher can be only partially phase-matched, and therefore the resulting mode can provide a corresponding helical phase-front only in the specific planes over the waveguide, separated by the beat length of the eigenmode superposition. In general, the numerical simulation results show that the beat length becomes larger for the farther away from cutoff propagation regimes. Despite such periodic behavior, this propagation regime could be yet applicable in the cases, when the vortex field should be used in a specific point, for example for the output to the free space beam or fiber. In order to tolerate the influence of fabrication uncertainty on the positions where the helical phase front can be formed, probably the thermo-optical effect can be used to provide the required phase shift between the constituent eigenmodes. Alternatively, if the integration platform allows p-type and n-type doping, the more efficient and fast management of the relative phases between eigenmodes can be achieved using the approach proposed in [61]. It exploits the plasma dispersion effect or Pockels effect in p-i-n phase shifters in order to modify the phase of the TE and TM modes together, or the TE modes independently, respectively. The question of efficient phase management in modal superpositions (1) is for further research.

In general, as the target azimuthal order increases and more eigenmodes are involved to the modal superposition, the effective index difference between the constituent eigenmodes becomes larger, and the beat length becomes correspondingly smaller. Moreover, even at the point $z = 0$, the normalized power of target OAM state decreases.

Acknowledgment

The authors would like to thank A. Shipulin, F. Küppers, G. S. Sokolovskii, V. E. Bougov, Xiaofeng Lu, and I. Tafur Monroy for fruitful discussions.

References

- [1] L. Allen, M. W. Beijersbergen, R. J. C. Spreeuw, and J. P. Woerdman, "Orbital angular momentum of light and the transformation of Laguerre–Gaussian laser modes," *Phys. Rev. A*, vol. 45, pp. 8185–8189, 1992.
- [2] M. J. Padgett, "Orbital angular momentum 25 years on," *Opt. Express*, vol. 25, no. 10, pp. 11269–11274, 2017.
- [3] J. Wang, "Twisted optical communications using orbital angular momentum," *Sci. China. Phys., Mech. Astron.*, vol. 62, no. 3, 2019, Art. no. 034201.
- [4] J. Wang *et al.*, "Multimode communications using orbital angular momentum," *Optical Fiber Telecommunications VIIB: Systems and Networks*. New York, NY, USA: Springer, 2013, pp. 569–615.
- [5] A. E. Willner *et al.*, "Optical communications using orbital angular momentum beams," *Adv. Opt. Photon.*, vol. 7, pp. 66–106, 2015.
- [6] A. Mair, A. Vaziri, G. Weihs, and A. Zeilinger, "Entanglement of the orbital angular momentum states of photons," *Nature*, vol. 412, pp. 313–316, 2001.
- [7] A. Nicolas, L. Veissier, L. Giner, E. Giacobino, D. Maxein, and J. Laurat, "A quantum memory for orbital angular momentum photonic qubits," *Nature Photon.*, vol. 8, pp. 234–238, 2014.
- [8] R. Fickler, R. Lapkiewicz, M. Huber, M. P. J. Lavery, M. J. Padgett, and A. Zeilinger, "Interface between path and OAM entanglement for high-dimensional photonic quantum information," *Nature Commun.*, vol. 5, 2014, Art. no. 4502.
- [9] D. J. Richardson, "New optical fibres for high-capacity optical communications," *Philos. Trans. R. Soc. A*, vol. 374, 2016, Art. no. 20140441.
- [10] A. D. Ellis, N. Mac Suibhne, D. Saad, and D. N. Payne, "Communication networks beyond the capacity crunch," *Philos. Trans. R. Soc. A*, vol. 374, 2016, Art. no. 20150191.
- [11] N. Bozinovic *et al.*, "Terabit-Scale orbital angular momentum mode division multiplexing in fibers," *Science*, vol. 340, pp. 1545–1548, 2013.
- [12] R. M. Nejad *et al.*, "Mode division multiplexing using orbital angular momentum modes over 1.4-km ring core fiber," *J. Lightw. Technol.*, vol. 34, no. 18, pp. 4252–4258, Sep. 15, 2016.

- [13] K. Ingerslev *et al.*, "12 mode, WDM, MIMO-free orbital angular momentum transmission," *Opt. Express*, vol. 26, no. 16, pp. 20225–20232, 2018.
- [14] M. Padgett and R. Bowman, "Tweezers with a twist," *Nature Photon.*, vol. 5, pp. 343–348, 2011.
- [15] K. Ladavac and D. G. Grier, "Microoptomechanical pumps assembled and driven by holographic optical vortex arrays," *Opt. Express*, vol. 12, no. 6, pp. 1144–1149, 2004.
- [16] M. P. Lavery, F. C. Speirs, S. M. Barnett, and M. J. Padgett, "Detection of a spinning object using light's orbital angular momentum," *Science*, vol. 341, pp. 537–540, 2013.
- [17] A. Ryabtsev, S. Pouya, A. Safarpour, M. Koochesfahani, and M. Dantus, "Fluid flow vorticity measurement using laser beams with orbital angular momentum," *Opt. Express*, vol. 24, no. 11, pp. 11762–11767, 2016.
- [18] S. W. Hell and J. Wichmann, "Breaking the diffraction resolution limit by stimulated emission: Stimulated-emission-depletion fluorescence microscopy," *Opt. Lett.*, vol. 19, no. 11, pp. 780–782, 1994.
- [19] M. Ritsch-Marte, "Orbital angular momentum light in microscopy," *Philos. Trans. R. Soc. A*, vol. 375, 2017, Art. no. 20150437.
- [20] V. Yu. Bazhenov, M. S. Soskin, and M. V. Vasnetsov, "Screw dislocations in light wavefronts," *J. Mod. Opt.*, vol. 39, no. 5, pp. 985–990, 1992.
- [21] N. R. Heckenberg, R. McDuff, C. P. Smith, H. Rubinsztein-Dunlop, and M. J. Wegener, "Laser beams with phase singularities," *Opt. Quant. Electron.*, vol. 24, no. 9, pp. S951–S962, 1992.
- [22] G. Gibson *et al.*, "Free-space information transfer using light beams carrying orbital angular momentum," *Opt. Express*, vol. 12, no. 22, pp. 5448–5456, 2004.
- [23] J. Wang *et al.*, "Terabit free-space data transmission employing orbital angular momentum multiplexing," *Nature Photon.*, vol. 6, pp. 488–496, 2012.
- [24] H. Huang *et al.*, "100 Tbit/s free-space data link enabled by three-dimensional multiplexing of orbital angular momentum, polarization, and wavelength," *Opt. Lett.*, vol. 39, no. 2, pp. 197–200, 2014.
- [25] N. Ahmed *et al.*, "Mode-division-multiplexing of multiple Bessel-Gaussian beams carrying orbital-angular-momentum for obstruction-tolerant free-space optical and millimetre-wave communication links," *Sci. Rep.*, vol. 6, 2016, Art. no. 22082.
- [26] Y. Ren *et al.*, "Spatially multiplexed orbital-angular-momentum-encoded single photon and classical channels in a free-space optical communication link," *Opt. Lett.*, vol. 42, no. 23, pp. 4881–4884, 2017.
- [27] V. V. Kotlyar, A. A. Kovalev, and A. G. Nalimov, "Energy density and energy flux in the focus of an optical vortex: Reverse flux of light energy," *Opt. Lett.*, vol. 43, no. 12, pp. 2921–2924, 2018.
- [28] S. N. Khonina, N. L. Kazanskiy, and V. A. Soifer, "Optical vortices in a fiber: Mode division multiplexing and multimode self-imaging," *Recent Progress in Optical Fiber Research*. London, U.K.: IntechOpen, 2012, pp. 327–352.
- [29] H. Huang *et al.*, "Mode division multiplexing using an orbital angular momentum mode sorter and MIMO-DSP over a graded-index few-mode optical fibre," *Sci. Rep.*, vol. 5, 2015, Art. no. 14931.
- [30] C. Brunet, B. Ung, L. Wang, Y. Messaddeq, S. LaRochelle, and L. A. Rusch, "Design of a family of ring-core fibers for OAM transmission studies," *Opt. Express*, vol. 23, no. 8, pp. 10553–10563, 2015.
- [31] H. Li *et al.*, "Orbital angular momentum vertical-cavity surface-emitting lasers," *Optica*, vol. 2, no. 6, pp. 547–552, 2015.
- [32] N. K. Fontaine, C. R. Doerr, and L. L. Buhl, "Efficient multiplexing and demultiplexing of free-space orbital angular momentum using photonic integrated circuits," in *Proc. Opt. Fiber Commun. Conf. Expo. Nat. Fiber Opt. Eng. Conf.*, 2012, Paper OTu11.2. 28.
- [33] D. Zhang, X. Feng, and Y. Huang, "Encoding and decoding of orbital angular momentum for wireless optical interconnects on chip," *Opt. Express*, vol. 20, no. 24, pp. 26986–26995, 2012.
- [34] T. Su *et al.*, "Demonstration of free space coherent optical communication using integrated silicon photonic orbital angular momentum devices," *Opt. Express*, vol. 20, no. 9, pp. 9396–9402, 2012.
- [35] J. Sun, A. Yaacobi, M. Moresco, D. Coolbaugh, and M. R. Watts, "Integrated continuously tunable optical orbital angular momentum generator," in *Proc. Conf. Lasers Electro-Opt.*, 2015, Paper JTh5A.5.
- [36] Y. Wang *et al.*, "Integrated photonic emitter with a wide switching range of orbital angular momentum modes," *Sci. Rep.*, vol. 6, 2016, Art. no. 22512.
- [37] X. Cai *et al.*, "Integrated compact optical vortex beam emitters," *Science*, vol. 338, pp. 363–366, 2012.
- [38] R. Li, X. Feng, D. Zhang, K. Cui, F. Liu, and Y. Huang, "Radially polarized orbital angular momentum beam emitter based on shallow-ridge silicon microring cavity," *IEEE Photon. J.*, vol. 6, no. 3, Jun. 2014, Art. no. 2200710.
- [39] Y. Wang *et al.*, "Generating optical superimposed vortex beam with tunable orbital angular momentum using integrated devices," *Sci. Rep.*, vol. 5, 2015, Art. no. 10958.
- [40] M. Scalfardi *et al.*, "3 × 3 optical switch by exploiting vortex beam emitters based on silicon microrings with superimposed gratings," *Opt. Lett.*, vol. 42, no. 19, pp. 3749–3752, 2017.
- [41] J. Liu *et al.*, "Orbital angular momentum modes emission from a silicon photonic integrated device for km-scale data-carrying fiber transmission," *Opt. Express*, vol. 26, no. 12, pp. 15471–15479, 2018.
- [42] J. Liu *et al.*, "Direct fiber vector eigenmode multiplexing transmission seeded by integrated optical vortex emitters," *Light Sci. Appl.*, vol. 7, 2018, Art. no. 17148.
- [43] S. Li *et al.*, "Orbital angular momentum vector modes (de)multiplexer based on multimode micro-ring," *Opt. Express*, vol. 26, pp. 29895–29905, 2018.
- [44] J. Zhang *et al.*, "An InP-based vortex beam emitter with monolithically integrated laser," *Nature Commun.*, vol. 9, 2018, Art. no. 2652.
- [45] D. Zhang, X. Feng, K. Cui, F. Liu, and Y. Huang, "Generating in-plane optical orbital angular momentum beams with silicon waveguides," *IEEE Photon. J.*, vol. 5, no. 2, Apr. 2013, Art. no. 2201206.
- [46] S. Zheng and J. Wang, "On-chip orbital angular momentum modes generator and (de)multiplexer based on trench silicon waveguides," *Opt. Express*, vol. 25, no. 15, pp. 18492–18501, 2017.
- [47] Y. Liang, H. W. Wu, B. J. Huang, and X. G. Huang, "Light beams with selective angular momentum generated by hybrid plasmonic waveguides," *Nanoscale*, vol. 6, pp. 12360–12365, 2014.

- [48] Y. Liang, F. Zhang, J. Gu, X. G. Huang, and S. Liu, "Integratable quarter-wave plates enable one-way angular momentum conversion," *Sci. Rep.*, vol. 6, 2016, Art. no. 24959.
- [49] Z. Ma, H. Chen, K. Wu, Y. Zhang, Y. Chen, and S. Yu, "Self-imaging of orbital angular momentum (OAM) modes in rectangular multimode interference waveguides," *Opt. Express*, vol. 23, no. 4, pp. 5014–5026, 2015.
- [50] B. Guan *et al.*, "Free-space coherent optical communication with orbital angular momentum multiplexing/demultiplexing using a hybrid 3D photonic integrated circuit," *Opt. Express*, vol. 22, no. 1, pp. 145–156, 2014.
- [51] S. J. B. Yoo, B. Guan, and R. P. Scott, "Heterogeneous 2D/3D photonic integrated microsystems," *Microsyst. Nanoeng.*, vol. 2, 2016, Art. no. 16030.
- [52] V. S. Lyubopytov *et al.*, "Optical vortex propagation in few-mode rectangular polymer waveguides," in *Proc. Opto-Electron. Commun. Conf. Photon. Global*, 2017, pp. 1–3.
- [53] V. S. Lyubopytov *et al.*, "Demonstration of optical vortex propagation in on-chip rectangular dielectric waveguides," in *Proc. Conf. Lasers Electro-Opt. Eur., Eur. Quantum Electron. Conf.*, 2017, Paper CI-3.2.
- [54] V. V. Kotlyar, A. A. Kovalev, and A. P. Porfirev, "Vortex Hermite–Gaussian laser beams," *Opt. Lett.*, vol. 40, no. 5, pp. 701–704, 2015.
- [55] E. Berglind and G. Björk, "Humblet's decomposition of the electromagnetic angular moment in metallic waveguides," *IEEE Trans. Microw. Theory*, vol. 62, no. 4, pp. 779–788, Apr. 2014.
- [56] T. E. Murphy, "Waveguide mode solver," 2006. [Online]. Available: <http://www.mathworks.com/matlabcentral/fileexchange/12734-waveguide-mode-solver>
- [57] A. B. Fallahkhair, K. S. Li, and T. E. Murphy, "Vector finite difference modesolver for anisotropic dielectric waveguides," *J. Lightw. Technol.*, vol. 26, no. 11, pp. 1423–1431, Jun. 2008.
- [58] E. A. J. Marcatili, "Dielectric rectangular waveguide and directional coupler for integrated optics," *Bell Syst. Tech. J.*, vol. 48, no. 7, pp. 2071–2102, 1969.
- [59] D. Marcuse, *Theory of Dielectric Optical Waveguides*, 2nd ed. San Diego, CA, USA: Academic, 1991.
- [60] E. Yao, S. Franke-Arnold, J. Courtial, S. Barnett, and M. Padgett, "Fourier relationship between angular position and optical orbital angular momentum," *Opt. Express*, vol. 14, no. 20, pp. 9071–9076, 2006.
- [61] N. Abadía *et al.*, "Highly fabrication tolerant InP based polarization beam splitter based on p-i-n structure," *Opt. Express*, vol. 25, no. 9, pp. 10070–1077, 2017.